Nanoparticle Therapeutics

Production Technologies, Types of Nanoparticles, and Regulatory Aspects

Edited by
Prashant Kesharwani, Kamalinder K. Singh

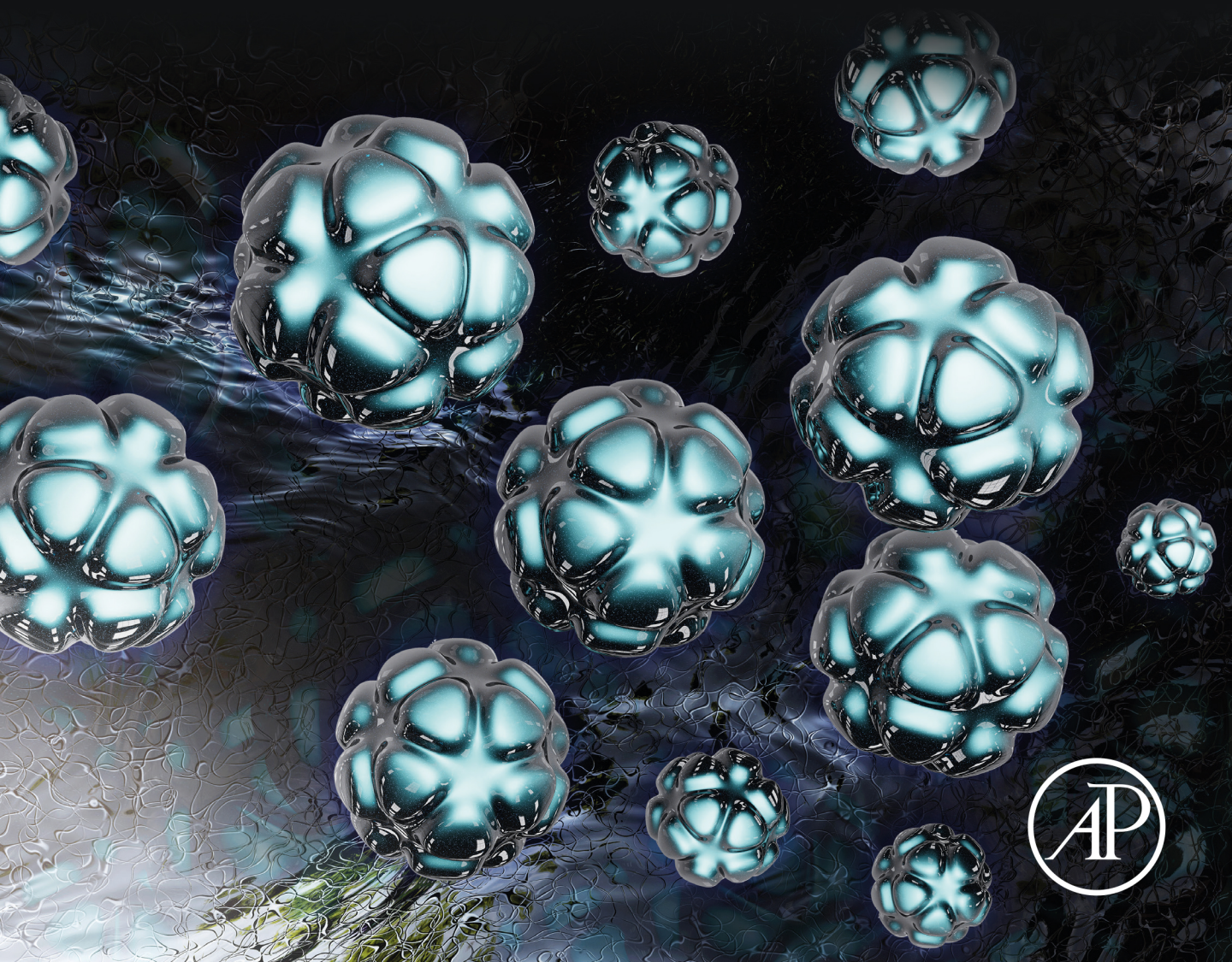

NANOPARTICLE THERAPEUTICS

Production Technologies, Types of Nanoparticles, and Regulatory Aspects

Edited by
PRASHANT KESHARWANI

KAMALINDER K. SINGH

ACADEMIC PRESS
An imprint of Elsevier

Academic Press is an imprint of Elsevier
125 London Wall, London EC2Y 5AS, United Kingdom
525 B Street, Suite 1650, San Diego, CA 92101, United States
50 Hampshire Street, 5th Floor, Cambridge, MA 02139, United States
The Boulevard, Langford Lane, Kidlington, Oxford OX5 1GB, United Kingdom

Library of Congress Cataloging-in-Publication Data
A catalog record for this book is available from the Library of Congress

British Library Cataloguing-in-Publication Data
A catalogue record for this book is available from the British Library

ISBN 978-0-12-820757-4

For information on all Academic Press publications
visit our website at https://www.elsevier.com/books-and-journals

Publisher: Stacy Masucci
Acquisitions Editor: Andre Gerhard Wolff
Editorial Project Manager: Timothy Bennett
Production Project Manager: Omer Mukthar
Cover Designer: Mark Rogers

Typeset by STRAIVE, India

CHAPTER 15

Radioactive nanoparticles and their biomedical application in nanobrachytherapy

Carla Daruich de Souza, Beatriz Ribeiro Nogueira, Carlos Alberto Zeituni and Maria Elisa Chuery Martins Rostelato
Laboratory for Radiation Therapy Sources Production, Nuclear and Energy Research Institute, National Nuclear Energy Commission, São Paulo, Brazil

1. Introduction

Nanotechnology is a new science. If the term nanoparticle was searched in ScienceDirect, in1996, only 623 papers were published. In 2006, the number increased to 7937. In September 2019, the number of papers published was almost 50,000 [1]. This rapid increase is certainly because of the huge potential of nanotechnology in different application fields. From biosensors to drug delivery, the nanoparticles can be applied to directly modify or receive information from systems and organs. This "new science" concentrates on the study of particles, structures, and materials that are in the nanoscale (nm) and have unique properties [2–4]. Their configuration in the nanometric size promotes alteration in their physical, chemical, and biological behaviors [3–5]. The quantum confinement effects state that the properties of materials are size-dependent in this scale range. In nanomaterials, the energy levels of the electrons are not continuous when compared to the bulk form. They are discrete due to the confinement of the electronic wave function in up to three physical dimensions, which leads to a change in surface area and electron confinement, making the changes in materials properties [3–5]. For example, properties such as melting point, fluorescence, electrical conductivity, magnetic permeability, and chemical reactivity change as a function of the size of the particle [3, 5]. Maybe the most important result of the nanoscale quantum effects is the ability to tune the properties. It means that a researcher can change the proprieties behavior to serve a determined purpose. For example, changing the fluorescence color of a particle can be used to identify diseases [4, 6, 7].

The surface chemistry of nanoparticles plays a direct role in the interactions between nanoparticles and biological systems can be altered by attaching molecules to the surface. As an example, charge, hydrophobicity, or even reactivity can be changed. Also,

Nanoparticle Therapeutics
https://doi.org/10.1016/B978-0-12-820757-4.00012-0

molecules of interest can be attached to their surface. For example, a chemotherapeutic drug can be encapsulated in a radioactive shell [8–10].

The union of brachytherapy with nanotechnology is inevitable. Brachytherapy is when a radiation source is placed in close contact or inside a patient's body. It can be left in the target area (TA) as a permanent seed implant, or it can treat the TA for a period of time. The primary use of brachytherapy is in the treatment of various types of cancers. It has the potential to be portable, due to the small size of the radiation sources. For example, iodine-125 seeds have 4.5 mm in length and 0.8 mm in diameter. Radioactive nanoparticles can be delivered by a syringe [11–13]. This is a major advantage of the method because it can be used in areas that people do not have access to large linear particle accelerators (linacs), which are expensive robust machines used in radiation therapy [14, 15].

The radiation dose received by the TA should be large enough to cause a lot of cellular damage, to the point of destruction. It needs to be focused on the TA as much as possible, saving the surrounding healthy tissues. Dose constraints are applied in all treatments and protocols are in constant review. Of course, since brachytherapy is placed inside the TA, it can focus even more on the target than EBRT (external beam radiation therapy), the other modality used for radiation therapy [13].

A radioactive nanoparticle would easily penetrate tumor vascularity and deliver radioactivity to the entire TA for enhanced effect. In the following part of the chapter, basics of radiation physics, radiological effects, factors to consider when creating a new brachytherapy modality, which nanosystems are promising, and the challenges that will be faced are explained.

2. Radiation concepts

When an atom has excess energy, that energy can be emitted in the form of radiation in several different forms. Basically, the atom nucleus will emit either particles or electromagnetic radiation. In radiation therapy, alpha, beta, gamma, and/or X-rays are used for treatment. Protons and neutrons are less used. Fig. 1 shows the alpha, beta, and X-ray/gamma radiation emission and the electromagnetic spectra [12, 16, 17].

Alpha decay typically occurs in very heavy nuclei, where electrostatic repulsion between protons in the nucleus is very large. The original radioactive isotope, also called father isotope (with an atomic number Z), emits its excess energy in the form of a helium nucleus (2 protons and 2 neutrons). The atom that remains, called daughter nuclei, has a Z-2 atomic number. The sum of the masses of the daughter nucleus and that of the alpha particle is slightly less than the mass of the father nucleus. Considering Einstein's $E = m^* c^2$, that mass difference is equivalent to the amount of energy released. They are usually very energetic and very heavy, thus have large ionization power and low penetration in matter [12, 16–19].

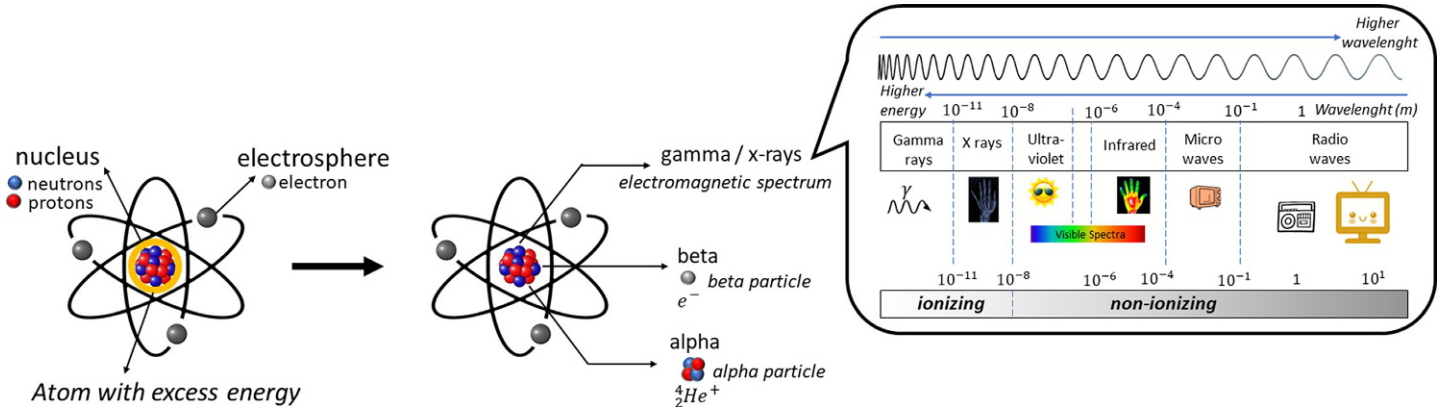

Fig. 1 Radioactive decay. When the atom has excess energy, the nucleus emits that energy in the form of radiation. Alpha emissions are actually a high-energy heavy helium atom nucleus. Beta emissions are a less heavy, less energetic electron. Gamma and X-rays are part of the electromagnetic spectra. They are from the same family as visible light, microwaves, and radio waves. The difference is in wavelength and ionization power.

In beta decay, a nucleus with too many protons or too many neutrons need to become stable. One of the protons or neutrons is transformed into the other. In beta minus decay (β^-), a neutron decays into a proton plus an electron and an antineutrino. In beta plus decay (β^+), a proton decays into a neutron plus a positron and a neutrino. To respect conservation laws, when an electrically neutral neutron becomes a positively charged proton, an electrically negative particle (electron in β^-) must be produced also. Because the electron mass is a tiny fraction of an atomic mass unit, the beta decaying nucleus mass is altered only by a very small amount. The core mass number does not change. Beta decay is, as a rule of thumb, less energetic than alpha emission and less heavy, thus have less ionization power but higher penetration in matter [12, 16, 17, 20, 21].

A gamma ray is when the nucleus changes from a higher energy state to a lower energy state through the emission of electromagnetic radiation (photons). The only thing that distinguishes a gamma ray from visible light photons emitted by a lamp is its wavelength. The gamma ray wavelength is hundreds of thousands of times smaller than that of visible light. Therefore, the frequency is hundreds of thousands of times greater. For complex nuclei of heavy elements, there are numerous different possibilities in which protons can rearrange themselves within the nucleus. Neither the mass number nor the atomic number of a nucleus changes when a gamma ray is emitted. However, the nucleus mass also decreases slightly and is converted into photon energy [12, 16, 17, 22, 23].

X-rays are produced by radiation interactions outside of the nucleus. Characteristic X-ray emission is when a moving electron hits an orbital electron with energy enough to remove it out of the inner electron shell of the target atom. After that, electrons from higher energy levels fill the vacancies, and X-ray photons are emitted. These X-rays have a discrete spectrum. Bremsstrahlung X-ray emission occurs when electrons are scattered due to the strong electric field near the nuclei. These X-rays have a continuous spectrum. The frequency of bremsstrahlung x-rays is limited by the energy of incident electrons [12, 16, 17].

Gamma decay and X-rays are, as a rule of thumb, less energetic than beta emission and they have no mass, thus have less ionization power but even higher penetration in matter [12, 16, 17].

Viewing all of this from the treatment standpoint, a few considerations need to be made. The first energy is deposited from the inside-out in brachytherapy. To concentrate the dose in the target and minimize the dose in the healthy surrounding tissues, a careful dosimetry study needs to be made. Energy should be high enough to reach the target but not as high to the point of causing necrosis to the healthy organs at risk (OAR). Fig. 2 presents radiation from both views [11, 13].

Radiation activity, half-life, and dose directly impact the treatment results. Activity is defined as the number of atoms that decay or emit their radiation, per second. This is measured in decay per second, or Becquerel (Bq). Activity after a period of time (A) depends on the initial activity (A_0) on the half-life ($T_{1/2}$) of the isotope used. Half-life

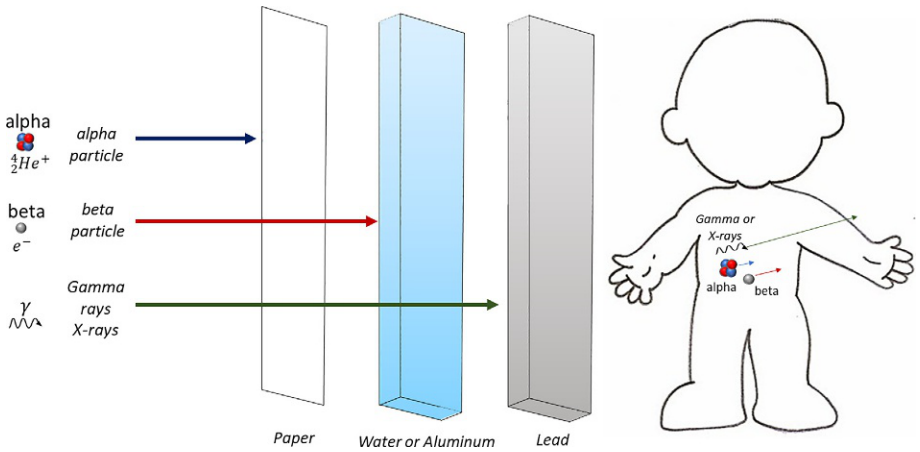

Fig. 2 Radiation penetration in matter from two standpoints: radiation source located outside the body, with examples of shielding materials; from inside the body.

is the time a radioactive source takes to emit half of the radiation. So, activity has an exponential behavior. Eqs. (1) and (2) shows the calculation [12, 16, 17].

$$A = A_0.e^{-\lambda.t} \tag{1}$$

or

$$N = N_0.e^{-\lambda.t} \tag{2}$$

where

A = final activity
A_0 = initial activity
N = final atoms number
N_o = initial atoms number
Decay coefficient: $\lambda = \frac{\ln 2}{T_{1/2.}}$
t = time

To know the necessary isotope mass to reach a certain activity, Eqs. (3) and (4) are used:

$$A = \lambda.N \tag{3}$$

$$m = \frac{M_a\, x\, N}{N_a} \tag{4}$$

where

A = activity needed
N = correspondent atoms number
M_a = atomic mass
N_a = Avogadro number
m = equivalent mass.

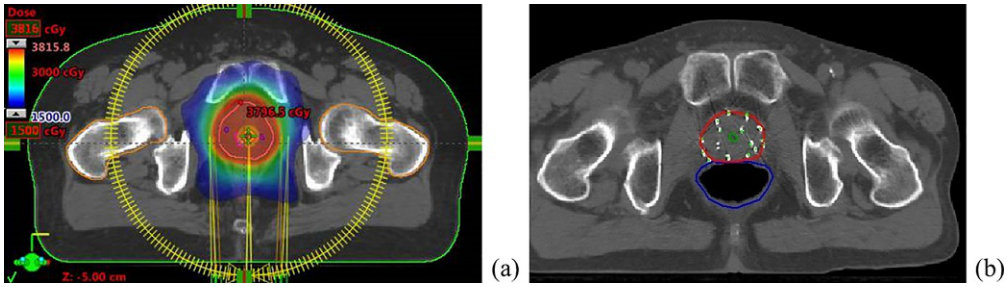

Fig. 3 Hiperfractionated EBRT (A) versus Brachytherapy planning (B) showing isodose curves. Notice that radiation deviates very little from the TA in brachytherapy.

The final dose would be calculated depending on treatment time. It is desirable that a high dose rate, higher activity, and energy in less treatment time are used. If a low dose rate is required, lower activity and energy in less treatment time is performed. The dose is the amount of energy released by the unit of mass. Usually, the unit Gy is used (equals to J/Kg). The higher the dose, the higher the effect. In a radiation therapy treatment, a dose chart is used to show where the cancer is, how much radiation is hitting it, and to quantify the dose in the OAR [11, 13]. Depending on the placement of the radiation source, the different organs with different intensities will be hit by radiation. Fig. 3 shows isodose curves for an Intensity Modulated Radiation therapy linac treatment versus a brachytherapy implant.

Radiation interacts with matter releasing the energy in the tissues. Basically, the energy is lost by two major routes: excitation or ionization. In excitation, which occurs in nonionizing radiation, the photon interacts with the atoms' electronsphere exciting electrons, but not strong enough to remove them. In ionization, energy is high enough to remove electrons. That is what occurs in ionizing radiation [24].

Since the human body is mostly water, radiation has a higher chance to hit a water molecule, creating free radicals. Those can cause cellular and DNA damage, killing the cell. There is also a chance that radiation directly hits the DNA strand causing mutations that can lead to cellular death. The amount of water directly impacts radiosensitivity, which will reflect on treatment radiation dose [24].

Another important aspect is angiogenesis. Cancer needs more blood supply to grow and, eventually, spread the damaged cells. To achieve this, it stimulates the growth of the vascular network [25]. It is proven that without good blood irrigation, tumors may become necrotic or even apoptotic [26, 27]. Radioactive nanoparticles could unite both forms of treatment: use radiation effects to kill cancer cells, use radiation effects to destroy tumor vascularity.

3. Necessary paths to develop nanobrachytherapy

To develop a new source, several factors must be considered. They will limit the radioisotopes that can be used.

The cancer site is very important. If the target area has more water and oxygen, more free radicals and oxygen reactive species will be formed, and the radiation effects will be greater. If the cancer is large, is likely the internal cells will be in anoxia, so treatment needs to be fractioned (killing the outside cells first, allowing the internal cells to restore, and then killing them with another radiation treatment fraction). If the cancer is aggressive, a higher dose rate may be necessary, all of which is limited by cancer location. In the case of the surrounding areas being sensitive, the dose must be restricted. For example, it is "easier" to treat prostate cancer than spinal cord cancer [12, 13, 28].

The way that the radioisotope is produced impacts final price and availability. If the isotope is produced naturally as part of the decay chain of uranium-238, uranium-235, or thorium-232, it is easily found (but high values can be spent with purification). If the isotope is a by-product of fission, it can be recovered from the nuclear fuel that has already been used. Only five countries in the world have facilities to reprocess spent fuel (England, India, France, Japan, and Russia). If the isotope needs to be produced in nuclear reactor or accelerator, costs can be high (due to the high cost of enriched targets) [28, 29].

Chemical stability, form, and waste management are also key. The radioactive material must be stable inside the body or the capsule. The decay product must do so also. For example, if a solid welded source decay product is gaseous, it might damage the structure. If a radiation source has a high half-life, it might be considered as a high-level waste after being used, needing management for a long period of time [12, 13, 28].

Energy, decay mode, radioactivity, and dose rate must be adequate to deliver the maximum amount of energy to the TA and minimum to the OAR. They must also not pose a threat to medical staff and the production operators. If manipulations require heavy shielding, the cost of treatment and manufacture is higher [12, 13]. Table 1 presents a few of the radioisotopes considered for use [28].

Dosimetry is important for all radiation therapy treatments. In brachytherapy, it depends on how the sources are positioned relative to the dose calculation points and on the source strength. The use of a well-established dosimetric system for the brachytherapy treatment of cancer needs to be established for each new source format and/or radioisotope used. However, the use of a model alone is not sufficient to validate results; reliability in source strength determination is necessary in order for the dose calculation to be accurate. Thus, brachytherapy sources need to be calibrated with traceability to a national or international standards laboratory. In situations in which the system to be used is not obvious, such as in nanobrachytherapy, all dosimetric modes must be investigated, and new models proposed [28].

Table 1 Radioisotopes used in brachytherapy and characteristics.

Radioisotope	Main emission type	Energy (MeV)	Half-life	Source format
Pd-103	X-rays	0.021	17 days	Seeds and nanoparticles
I-125	γ, X-rays	0.035, 27.4	59.6 days	Seeds
Ir-192	β^-, γ	0.29 and 0.16, 0.32	74 days	Wire, pellets, and seeds
P-32	β^-	0.695	14.29 days	Plaques
Cs-131	X-rays	0.030	9.7 days	Seeds
Au-198	β^-, γ	0.31, 0.41	2.7 days	Nanoparticles
Ru-106 (decays to Rh-106)	β^- β^-	0.04 1.5	1.02 years 30 s	Plaques
Lu-177	β^-	0.149	6.64 days	Nanoparticles
Y-90	β^-	2.28	64 h	Plaques
In-111	β^- X-rays	0.245 and 0.171 0.023	2.8 days	Nanoparticle coatings

Next, the patient and source production journey will be summarized (basic steps). When a patient with cancer enters a radiation therapy center, the medical staff will evaluate a 3D computed tomography (CT). If brachytherapy is recommended, treatment planning starts. Let us suppose that iodine-125 sources will be implanted inside the prostate. The staff will perform a mock-up treatment in the planning system (TPS), a software containing all information from the patient and radiation source. This will consider the patient's prostate anatomy and will inform the staff approximatively how many sources needed to be used for treatment success (80–120). Accessories that maybe be used (such as immobilizers, extra shielding, and others) are also determined. The purchase order is relayed to the manufacturer. Inside the industrial radioactive plant, a hot cell (completely shielded and airtight led structure) is used in production. The iodine-125 seed can have many configurations that impact production. Let us consider the most used: silver core that contains the radioactive material surrounded by a titanium capsule. The production for the patient seeds starts by performing the chemical iodine-125 binding reaction to the core. Then, the radioactive core is placed inside a titanium capsule that is then welded in both ends. Leakage tests are performed to ensure weld success. Radioactivity is measured to confirm the correct value. The order is filled. The TPS already has all the information about the source dosimetry. That information was obtained in a study made before the seed even reach the medical market. Dosimetry methods, such as calculations according

to protocols (AAPM TG-43 for iodine-125 [30]), thermoluminescent dosimeters (such as TLD-100), film, Monte Carlo simulations (AAPM TG-186 [30]), in vitro and in vivo dosimetry, among others, should be already performed. The seeds reach the hospital after authorized transport to the hospital. Source activity is calculated to reach the desired value at the time of the implant. Depending on distance, they might leave the manufacturing site with more radioactive activity to compensate for decay. After the implant is performed, a dose curve is calculated by the TPS, like the example shown in Fig. 3B.

This example is here to show the difficulties of developing and implementing a new form of treatment in the radiation therapy field. A lot of investment in manufacturing, calibration, quality insurance, transport logistics, software development, training, hospital operation room needs to be made.

For nanobrachytherapy, we are still in the early developing stages. Efforts are still in synthesis methods, validation in cell and animal models, and dosimetry models propositions. Mostly, gold-198 and palladium-103 nanoparticles are being explored.

The pathway to developed radioactive nanoparticles also depends on if the technique can be reproduced nonradioactively. Most of the characterization cannot be performed with the radioactive product due to the risk of contamination. Also, the equipment needs to be in a controlled area with all radiation protection measurements in place. Usually, DLS (Dynamic light sizer), Zeta Potential, FTIR (Fourier Transform Infrared Spectroscopy), and UV-vis (UV-Visible Spectroscopy) are possible to access the radioactive product (that, of course, depends on the equipment characteristics). However, TEM (Transmission electron microscopy), AFM (Atomic Force Microscope), CP-MS (Inductively coupled plasma mass spectrometry), and NMR (Nuclear Magnetic Resonance) cannot be used. The synthesis technique must also consider this contamination issue. If a unique glassware, rotary evaporator, shakers, centrifuge, HPLC (High performance liquid chromatography) is being used to produce and refine the nonradioactive product, the radioactive route might not be possible.

3.1 Nanoparticle synthesis

Nanoparticles can be synthesized by several routes (Fig. 4). Usually, nanoparticle type, final use, and equipment availability are determinant factors when choosing a method. For radioactive nanoparticles, simplicity must be pursued when performing the synthesis. Choosing a method that needs an expensive machine, high heating, or has volatilization is unfeasible.

Radioactive nanoparticles for cancer treatment are mainly being synthesized by chemical reduction (CR). It is a simple route that only needs basic lab glassware and a chemical reducing agent to form nanoparticles. In Fig. 5, the most used CR pathways are presented.

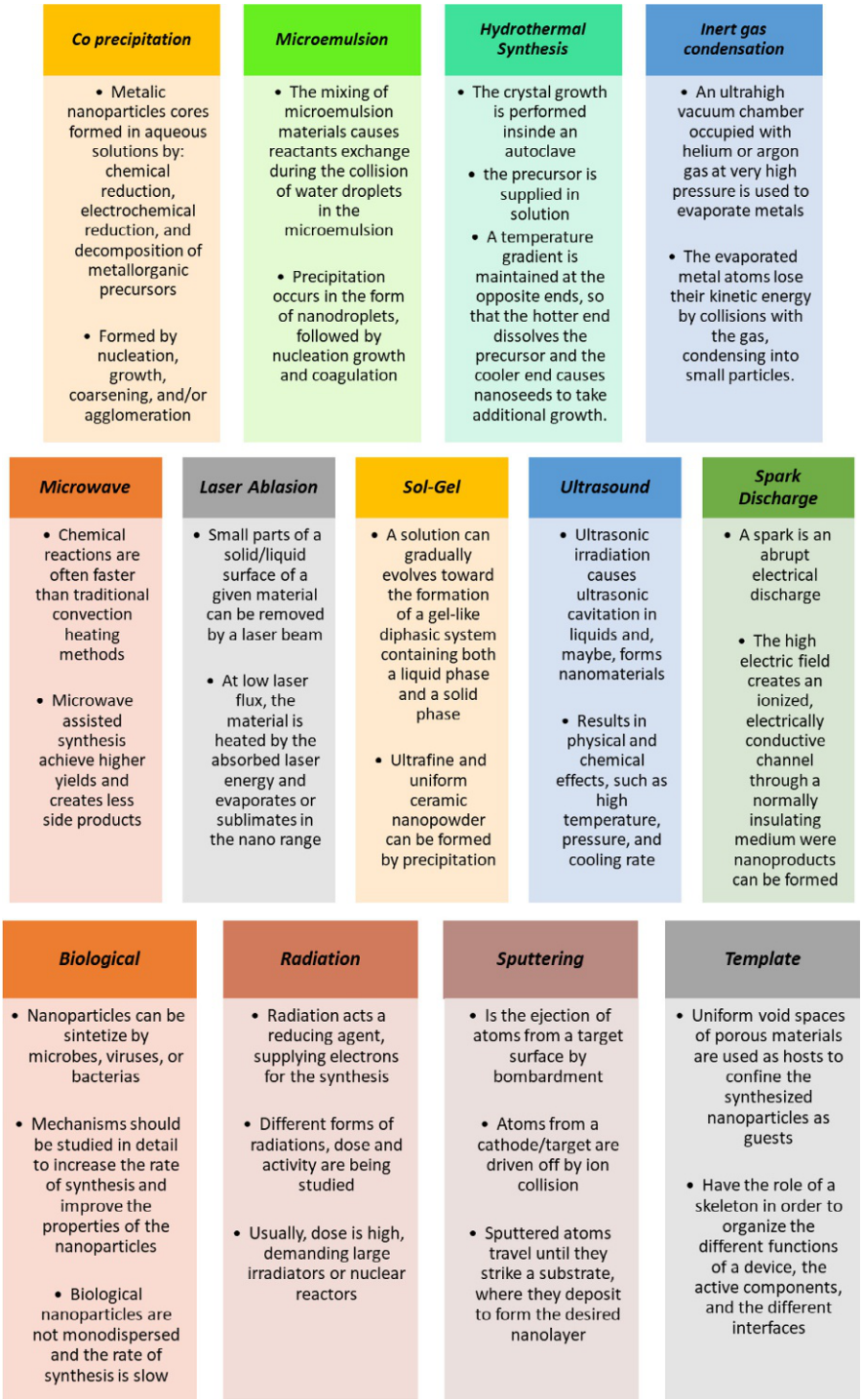

Fig. 4 Summary of the main methods used in the synthesis of nanoparticles. Information from [31].

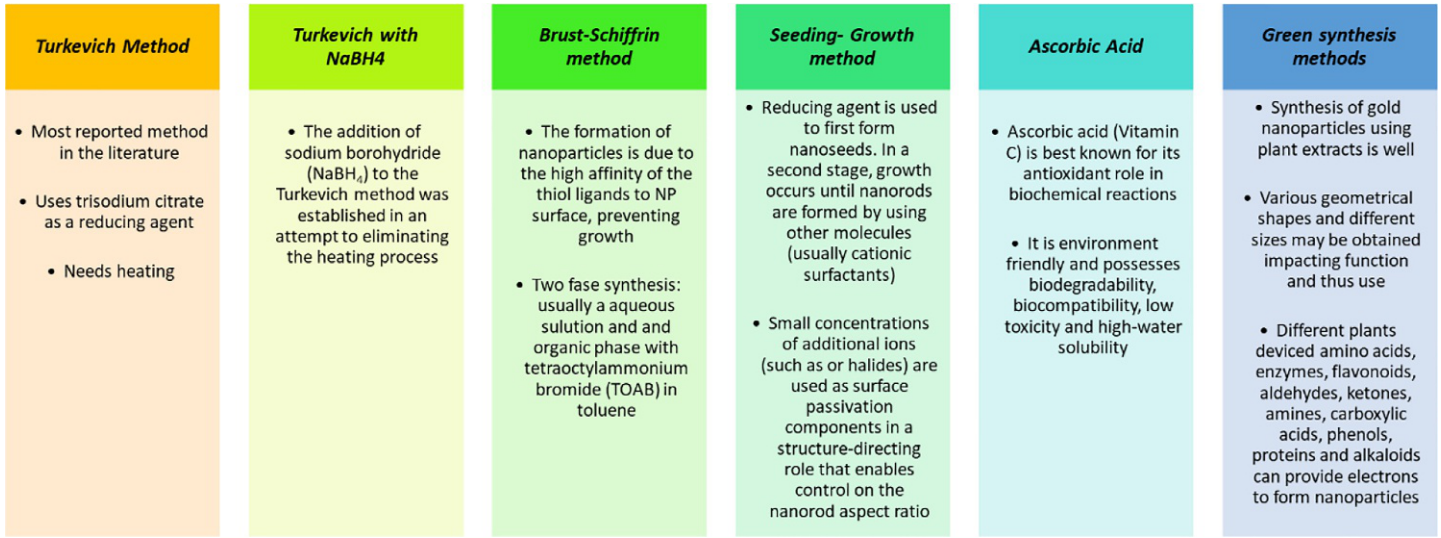

Fig. 5 Summary of the main methods used in the synthesis of gold nanoparticles. Information from [3].

For successfully synthesized nanoparticles, the aggregation barrier (activation energy that two particles have to overcome to merge into one) increases to an optimum particle size allowing colloidal stability to be reached. The steps are presented below [32]:

Step 1: High reduction rate increases the number of particles. Clusters with 1–2 nm are formed.

Step 2: Reduction continues at a much lower rate. Since particles have weak stabilization at this stage, coalescence processes take place (two or more droplets, bubbles or particles merge during contact to form a single daughter droplet, bubble, or particle), resulting in a decrease in the number of particles. When the radius is around 2.5 nm, the number of particles is now constant, but they keep growing in size.

Step 3: NPs grow due to the diffusion of the metal atoms reduced in the solution.

Step 4: When the particles reach a radius of around 4–5 nm, the growth rate increases drastically and the remaining metal salt is consumed. Particle size increases to the final radius.

Synthesis routes for the preparation of gold nanoparticles are presented in Fig. 5 and elaborated below:

(a) *Turkevich method:* 95 mL of $HAuCl_4$ solution (containing 5 mg Au) was heated to the boiling point and 5 mL of 1% sodium citrate solution was added to the boiling solution with good mechanical stirring. The reaction mixture was colorless for 12 s after the addition of the citrate, and then it turned purplish-blue within a fraction of a second. After 5 min, the final color was deep wine red. The best results were obtained with 5–50 mg citrate addition. The particle size achieved 20 nm. [33]

(b) *Turkevich method with $NaBH_4$*: 1 mL of 1% $HAuCl_4$ was added to 90 mL of H_2O at room temperature. After 1 min of stirring, 2.00 mL of 38.8 mM sodium citrate was added. One minute later, 1.00 mL of fresh 0.075% $NaBH_4$ in 38.8 mM sodium citrate was added. The colloidal solution was stirred for an additional 5 min and stored in a dark bottle at 4°C. Particles had 13 nm [34, 35].

(c) *Brust-Schiffrin method*: $HAuCl_4$ (30 mL, 30 mM) was mixed with a solution of tetraoctylammonium bromide (TOAB) in toluene (80 mL, 50 mM). The two-phase mixture was vigorously stirred until all the tetrachloroaurate was transferred into the organic layer and dodecanethiol (170 mg) was then added to the organic phase. A freshly prepared aqueous solution of sodium borohydride (25 mL, 0.4 M) was slowly added with vigorous stirring. After further stirring for 3 h, the organic phase was separated, evaporated to 10 mL in a rotary evaporator, and mixed with 400 mL ethanol to remove excess thiol. The mixture was kept for 4 h at −18°C, and the dark brown precipitate was filtered off and washed with ethanol. The crude product was dissolved in 10 mL toluene and again precipitated with 400 mL ethanol. Particles produced by this method reached 2.5 nm [36, 37].

(d) Seeding-growth method:

(i) Seed solution—20 mL aqueous solution containing 2.5×10^{-4} M $HAuCl_4$ and 2.5×10^{-4} M trisodium citrate was prepared in a conical flask. Next, 0.6 mL of ice-cold, freshly prepared 0.1 M $NaBH_4$ solution was added to the solution while stirring. The solution turned pink immediately after adding $NaBH_4$, indicating particle formation. The particles in this solution were used as seeds within 2–5 h after preparation. Citrate serves only as a capping agent since it cannot reduce the gold salt at room temperature (25°C). [38]

(ii) For the growth solution, a 200 mL aqueous solution of 2.5×10^{-4} M of $HAuCl_4$ was prepared in a conical flask. Next, 6 g of solid cetyltrimethylammonium bromide (CTAB- 0.08 M) was added to the solution, and the mixture was heated until the solution turned a clear orange color. The solution was cooled to room temperature and used as a stock growth solution [38].

(iii) Several routes were successful to produce various-sized gold nanoparticles by mixing different quantities of the seed and growth solutions. For example, 7.5 mL of growth solution was mixed with 0.05 mL of freshly prepared 0.1 M ascorbic acid solution. Next, 2.5 mL of seed solution was added while stirring. Stirring continued for 10 min after the solution turned wine red. Particles prepared this way were spherical with a diameter of 5.5 nm [38].

(e) *Ascorbic Acid method:* 10^{-2} M gold salt (200 mL) was mixed with 20 mM ice-cold ascorbic acid (70 mL) under continuous stirring. The temperature of the reaction synthesis was maintained to 4°C throughout. With the addition of gold salt, the colorless solution of ascorbic acid is changed to purple and finally faint blue. The average size of nanoflowers was measured to be of the order of 45 nm, the core size is around 35 nm, and the length of the petals is around 5 nm [39].

(f) *Green synthesis:* Different compositions and quantities of reducing agents are found in organic extracts can be used to produce NPs. CH-AuNPs were synthesized by using biopolymer chitosan for the reduction of gold salt. For preparation, 500 μL of a freshly prepared solution of chitosan (8 mg/mL) dissolved in 1% acetic acid solution was added to 10 mL of 1 mM tetrachloroauric acid ($HAuCl_4$) solution and stirred at 70°C until the color changed from pale yellow to red, which indicates the nanoparticle formation. Gold NPs had a narrow size distribution with an average size of 10–15 nm [40].

During the NPs fabrication process, the coordination sites of the surface atoms are not complete, allowing the binding of donor-acceptor species, or ligands. These molecules are easily bound to the surface establishing a double layer of charge that prevents nanoparticle aggregation. This coating agent can also be functionalized to provide reactive groups, such as amines, for subsequent modification [10].

Surfactants can be used to control the growth of nanomaterials to achieve desired morphologies [41]. At low concentration, those amphiphilic substances can be adsorbed on surfaces or interfaces resulting in an alteration of free energy available resulting in well-dispersed NP solutions [42].

3.2 Gold-198 nanoparticles, Au^{198}NPs

In the beginning, brachytherapy was limited to only Radium-226 and Radon-222. However, due to complications associated with high energy emissions from radium [43], gold-198 was introduced as an option by Flocks et al. from Iowa State University in 1951. They treated 400 men with inoperable prostate cancer and shown significant palliative results [44]. Today, it is still being used to treat an array of cancers, such as prostate, in different formats, such as seeds, foils, and pellets [45].

Gold nanoparticles were the first to be described in the literature. They were used as a method for staining glass to a wine-red color. The Lycurgus Cup, manufactured in 4th-century Rome, changes color depending on the location of the light source [46]. When the light source is transmitted, glass turned red by the addition of a precious metal-bearing material when the glass was molten. Now it is known that the color change is because of gold and silver nanoparticles [46].

AuNPs have small gold particles with a diameter of 1–100 nm, which, once dispersed in water, are also known as colloidal gold. Functionalized gold nanoparticles are the subject of intensive studies and biomedical applications [47], including genomics [48], biosensors [49], immunoassays [50], clinical biochemistry [51], laser phototherapy of cancer cells and tumors [52], the targeted delivery of drugs [53], optical bioimaging [39], and monitoring of cells and tissues [54].

Faraday [55] presented in 1857 the first synthesis methodology with a scientific eye. He used chloroauric acid ($HAuCl_4$) as a precursor and a phosphorus-ether solution as a reducing agent. The solution turned first brown, then gray, purple, and red, finally giving a deep-red product. He had produced extremely fine particles with a mean diameter of 50 Å (5 nm).

Oxidation states of gold are Au^{+1} (aurous), Au^{+3} (auric), and its nonoxidized state Au^0. Au^0 is the final electric state found in nanoparticles. Therefore, the synthesis of AuNPs is actually a reduction from Au^{+1} or Au^{+3} states to Au^0 using an electron donor (reduction agent). The precursor of choice for the majority of researchers is chloroauric acid, $HAuCl_4$ with gold in its Au^{+3} oxidation states. [3, 5, 56]

Gold in colloidal form has been used since the 1950s. The research group led by P. Hahn (Meharry medical college, Nashville-TN, USA) had used gold-198 in several types of cancer, such as leukemia and lung cancers [57–59]. In 1949, Miller's group located in Switzerland proposed an injection of colloidal radioactive gold directly into the body cavity as an effective way to treat cancer [60]. The research in the field became scarce with the development of EBRT cobalt units and, later, linacs.

Nanoparticles are generally produced by reducing tetrachloroauric acid with various agents such as borohydride, amines, alcohols, carboxylic acids, sodium citrate, sodium borohydride, ascorbic acid, and others (examples in [61, 62]). At the same time, small organic molecules or polymers should/can be added to the system to prevent the aggregation of the formed nanoparticles. The final shape achieved is generally spherical [3, 63].

The major question is: Can tetrachloroauric acid be placed inside a nuclear reactor and only gold be activated? If no, can it be fabricated from radioactive pure gold? The answers are: no and yes. Chlorine forms a high energy high half-life isotope making it impossible to use inside a human body. Gold foils or wires can be turned into $HAu^{198}Cl_4$ by being dissolved with aqua regia.

Aqua Regia dissolves gold, though neither HCl nor HNO_3 has the power to dissolve it alone, because, in combination, each acid performs a different task. Nitric acid is a powerful oxidizer, which dissolves a virtually undetectable amount of gold, forming ions of gold (Au^{3+}). The hydrochloric acid provides chloride ions (Cl^-), which react with the ions gold to produce tetrachlorourate (III) anions, also in solution. The reaction with hydrochloric acid is an equilibrium reaction that favors the formation of chlorourate anions ($AuCl_4^-$). This results in the removal of gold ions from the solution allowing further oxidation of the remaining gold. The gold foil then becomes chlorouronic acid [3, 64].

To produce gold-198 a nuclear reactor is necessary. Highly pure gold (99.99 +%) is placed in the reactor neutron flux. The core becomes unstable, radioactive. Stable gold (197 in mass) turns into radioactive gold-198. After emitting beta radiation with 314.55 keV and gamma with 411.8 keV, the remaining atom is now stable mercury with 198 mass [65]. Eq. (5) summarizes gold-198 formation and decay.

$$^{197}_{79}\mathrm{Au} + {}^{1}_{0}\mathrm{n} \xrightarrow{98.65\ \text{barns}} {}^{198}_{79}\mathrm{Au} \xrightarrow[\gamma,\beta^-]{} {}^{198}_{80}\mathrm{Hg} \tag{5}$$

In order to estimate the final activity, the following calculation is used (Eq. 6) [17]. Explanation of Eq. (6) indexes can be found in Table 2.

$$A = \frac{M.N.\theta.\sigma.\phi}{P}\left(1 - e^{-\lambda t}\right) \tag{6}$$

Next, we will present the advance in ^{198}AuNPs reported in the literature.

Table 2 Initials meaning for Eq. (1).

Initial	Meaning	Unity
A	Activity	Bequerel
P	Atomic weight	g/mol
M	Mass	g
N	Avogadro	6.02×1023
θ	Isotopic abundance	%
λ	Decay	$time^{-1}$
ϕ	Reactor flow	$n\,cm^2/s^{-1}$
σ	Cross section	cm^2 [a]
t	Irradiation time	time

[a] $1\,barn = 10^{-24}\,cm^2$.

The group headed by K. Katti (University of Missouri, EUA) developed a gold-198 nanoparticle coated with gum arabica [62]. The authors state that their new method is better than the classic ones that consisted in the reduction of Au^{3+} in $AuCl_4^-$ with $NaBH_4$ or sodium citrate, compounds that the author claims are highly toxic. Instead of the traditional route, the researchers synthesized a novel reducing agent that was named THPAL-alanine trimeric with phosphines. The amount 0.500 g, 4.033 mmol of Tris(hydroxymethyl)phosphine (THPAL) in 5 mL of distilled water was added dropwise to (L)-Alanine/(D)-Alanine (1.077 g, 12.00 mmol) in 10 mL of distilled water at 25°C. The reaction mixture was stirred under dry nitrogen for 1 h. The solvent was removed in vacuo to obtain a white solid. The white solid was washed with methanol and dried in vacuo to give the pure product (L)- or (D)- in 90% yield. For $H^{198}AuCl_4$ fabrication, the research group conveys two routes:

(a) $^{198}AuCl_4^-$ was activated in a nuclear reactor with a flow of $8x10^{13}n/cm^2/s$ in an acid solution of HCl [62].

(b) Au-198 was produced by direct irradiation of natural gold foil or metal Au-197(n,γ) Au-198. Gold foil was irradiated at a neutron flux of $8 \times 10^{13}\,n/cm^2/s$. After irradiation, the radioactive foil was dissolved with aqua regia, dried down, and reconstituted in 0.05–1 mL of 0.05 N HCL to form $H^{198}AuCl_4$ [66].

Gum arabica was used as a coating stabilizing agent. It consists of a mixture of lower molecular weight polysaccharides and higher molecular weight hydroxyproline-rich glycoprotein. Stability studies carried out with AuNPs have demonstrated that the saccharide and protein structure provides exceptional stability for AuNPs for periods of over six months. Therefore, we have selected gum arabica stabilized ^{198}AuNPs for further in vivo pharmacokinetic studies [66].

After activation, 50–100 μL of $H^{198}AuCl_4$ is added with 6 mL of gum arabica along with 20 μL/0.0337 THPAL for each mL of solution. This reaction occurs results in radioactive gold nanoparticles in less than 5 min.

The analysis of the material, without the radioactive nucleus, was performed obtaining the following results: DLS mean diameter: 7 ± 3 nm, TEM mean diameter: 17.5 ± 2.5 nm, DLS average diameter (with gum arabica coating): 85 nm, zeta potential: -24.5 ± 1.5 mV, and UV-Vis plasmon absorption band: 540 nm. In vitro tests obtained the following results. Biological stability test performed with 10% NaCl, 0.5% cysteine, 0.2 M histidine, 0.5% HSA (human serum albumin), and various pH values were found to be stable without aggregation or decomposition. The Hemocompatibility test did not result in hemolysis and the platelet aggregation test showed that the function was inhibited or cause platelet aggregation.

The biodistribution studies were performed in normal, SCID [62] and CF-1 [66] mice. They were then euthanized, and the tissues and organs were excised from the animals following at 1 h, 4 h, and 24 h postinjection. Subsequently, the tissues and organs were weighed and counted in a NaI well counter. Two varieties were reported, yielding

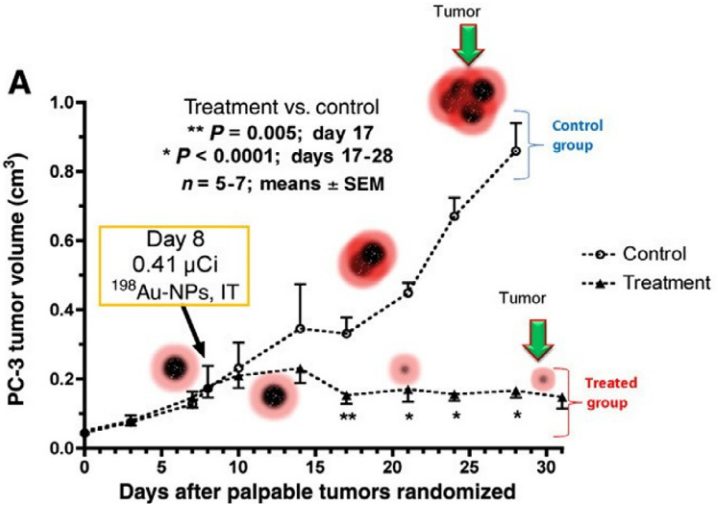

Fig. 6 Therapeutic efficacy of GA-^{198}AuNPs in prostate tumor-bearing mice. *(Reproduced from N. Chanda, et al., Radioactive gold nanoparticles in cancer therapy: therapeutic efficacy studies of GA-198AuNP nanoconstruct in prostate tumor-bearing mice. Nanomedicine 6 (2) (2010) 201–209 with permission. Elsevier RightsLink: 4,680,770,734,640.)*

the following results: 408 μCi nanoparticles were injected directly into cancer (PC3 prostate cancer cells) and remained for three weeks. After two weeks, 19.9% of the injected dose was found in the tumor, 0.91% in the liver, 0.13% in the kidney, 0.09% in the intestine, and 18.5% in the carcass [62]. On euthanasia of the animals, a reduction of up to 82% of the size of the cancer was observed (Fig. 6).

10–20 μCi nanoparticles were injected directly tail vein (20–40 μL). The pharmacokinetics and biodistribution studies of gum arabica (glycol protein) coated 198-AuNPs in mice showed >80% uptake in the liver with minimal accumulation in blood and other non-target organs. Authors suggest the use in liver cancer [66]. Red blood cell, platelet, lymphocyte, and antibody count remained the same as in healthy animals for both experiments.

The same research group developed gold-198 nanoparticles coated with epigallocatechin-gallate (EGC) as an alternative treatment for prostate cancer treatment [67]. An advantage of EGC is its ability to target the Laminin receptor (Lam 67R) that is over-expressed in human prostate cancer cells [68]. The authors initially synthesized the non-radioactive surrogate EGC-AuNP by mixing sodium tetrachloroaurate ($NaAuCl_4$) with EGC in deionized water [67]. For EGC-^{198}AuNPs, a 0.76 mg gold leaf was irradiated for 3.5 h (no extra information on the nuclear reactor characteristics was provided). The calculated activity achieved was 20.5 mCi. The now radioactive foil was dissolved in 800 μL of aqua regia. The solution was heated until the volume reaches approximately 200 μL. Then 600 μL of 0.05 M HCl was added and heating continued until most of the

acid had evaporated. The solution was then allowed to cool followed by the addition of 200 μL of 0.05 M HCl. A 0.17 mg/mL solution of EGC was prepared under constant stirring at 25°C for 3 min. To this solution, 2 μL of $H^{198}AuCl_4$ (0.41–1.3 mCi) and 98 μL of 0.1 M $NaAuCl_4$ carrier solution were added. The wine-red expected color change occurred after 5 min. The reaction mixture was stirred for an additional 15 min at 25°C [67]. Probably, the carrier solution formed EGC-Au:^{198}AuNPs.

Characterization, in vitro, and in vivo studies were performed with the non-radioactive version. The nanoparticles showed particle size of 125 ± 5 nm with DLS while TEM of the core nanoparticles without the EGC layer demonstrated a mean diameter of 47.5 ± 7.5 nm and zeta potential of −37.7 mV with UV-Vis plasmon absorption band: 535 nm. The hemocompatibility assay involved direct exposure of EGC-AuNP to freshly drawn whole human blood for 2 h at 25°C. The results obtained confirmed that the EGC-AuNP remained intact. A size variation of 10 nm (monitored through changes in surface plasmon resonance—UV-Vis) when tested in presence of with 10% NaCl, 0.2 M, histidine, 0.5% human serum albumin (HSA), 0.5% Bovine Serum Albumin (BSA), and at various pH values. No detectable aggregation/decomposition was noted in EGC-AuNPs when assessed by incubating the nanoparticles in cell culture media.

SCID mice received intratumoral injections of EGC-^{198}AuNP (3.5 μCi) in DPBS (20 μL) while performed under brief inhalational anesthesia. Analysis of ^{198}Au radioactivity revealed that 72.4 ± 5.9% was retained in prostate tumors at 24 h. Slow clearance (leakage) into the blood with only 0.06% at 24 h was observed. Lungs and pancreas exhibited low uptake at 24 h, with only 0.33% and 0.22%, respectively.

Cancer size and treatment progression are shown in Fig. 7. The end-of-study biodistribution on Day 42 showed that 37.4 ± 8.1 of EGC-^{198}AuNP remained in the residual tumor, while 17.8 ± 6.1 was noted for carcass and 2.5 ± 1.7% was observed in the liver. Retention in other tissues was negligible, with radioactivity near background levels for blood, heart, lung, spleen, intestines, stomach, bone, brain, and skeletal muscle.

In comparison, EGC-^{198}AuNP was retained in tumors for more than twice time period when compared to GA-^{198}AuNPs.

Efforts continue with new research continuing being done in synthesis, validation, and dosimetry approach.

3.3 Palladium-103 nanoparticles (Pd^{103}NP)

Palladium-103 brachytherapy was introduced in 1987 as an alternative to iodine-125, also suitable for interstitial implantation. The characteristics of palladium-103 are similar to iodine-125 in that it emits a low-energy photon with an average energy of 21 KeV. The shorter half-life of palladium-103 (17 days), relative to that of iodine-125 (60 days), results in a higher initial dose rate [69]. They are being used mostly for prostate cancer in the seed form.

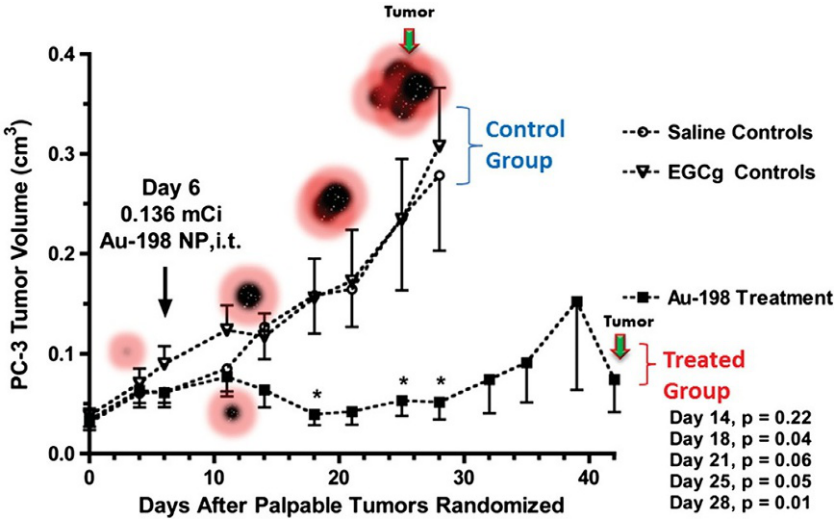

Fig. 7 Therapeutic efficacy of EGC-^{198}AuNPs in prostate tumor-bearing mice. *(Reproduced from R. Shukla, et al., Laminin receptor specific therapeutic gold nanoparticles (^{198}AuNP-EGCg) show efficacy in treating prostate cancer, Proc. Natl. Acad. Sci. U. S. A. 109 (31) (2012) 12426–31 with permission.)*

Palladium nanoparticles are used as catalytic materials [70] (due to high surface-area-to-volume ratio), hydrogen storage [71], sensing [72], and more recently as radioactive nanoparticles for cancer treatment. Their synthesis can follow chemical or electrochemical methods using a variety of stabilizers including organic ligands, salts/surfactants, polymers, and dendrimers [73]. The palladium precursor used can have an important impact on the nanoparticles formed. The Pd(acetylacetonate)$_2$ salt gave more monodispersed distributions than the corresponding nitrate or chloride salts [74]. This is maybe due to carbon monoxide molecules being formed by the decomposition of the acetylacetonate [75].

By far the most common synthesis direction is to use ligands. They are also successful in avoiding agglomeration. Sulfur-based ligands, such as thiols, acting as electron donors, are highly efficient stabilizers due to strong interactions with Palladium (and other metals). The method developed in the 1990s by Brust-Schiffrin [37] is based that metal salt is dissolved in water and first transferred to the organic phase using a suitable phase-transfer agent, such as tetraoctylammonium bromide (TOAB). Then, an aqueous sodium borohydride solution is added to the stirred biphasic system, leading to the formation of nanoparticles. The ratio of metal to organo-thiol and the reaction temperature control particle size. The nanoparticles, protected by a compact shell of organo-thiols, are stable for long periods of time, either in solution or as solids that can be readily redispersed in organic solvents [3, 37, 74]. To synthesize small nanoparticles, the use of long thiols in excess with an additional quantity of reducing agent will increase reaction yield [74].

The Brust-Schiffrin pathway has successfully been used to prepare palladium nanoparticles stabilized by simple lipophilic *n*-alkanethiols. The two-phase methodology allows easy nanoparticle separation from the aqueous by-products. However, when more polar ligands are used, the purification can get more complicated [74].

An alternative synthesis route that allows a wider variety of ligands to be used was presented by Yee et al. [76]. Superhydride (lithium triethylborohydride, $LiEt_3BH$) was used as a reductant agent. The combination of palladium (II) acetate with octadecanethiol resulted in a soluble metal-thiolate complex in tetrahydrofuran (THF). The addition of superhydride solution to this resulted in stable nanoparticles being formed with an average diameter of 2.3 nm [74, 76].

Another strategy for preparing palladium nanoparticles soluble in aqueous systems is to use ω-substituted thiol ligands (contains a charged functional group, such as ammonium or carboxylate salts). The sodium borohydride reduction of potassium tetrachloropalladate(II) in the presence of the chloride salt of the *N*,*N*-trimethyl(undecylmercapto)ammonium ligand in a one-phase system results in water-soluble PdNPs with an average diameter of 2.7 nm [74, 77].

The use of phosphine ligands has also been used for palladium nanoparticle preparation. Kim et al. [75] used thermolysis of palladium-trioctlyphosphine (TOP) complex to synthesized nanoparticles. Nanoparticles with 3.5 nm were formed when Palladium (acetylacetonate)$_2$, and TOP were heated to 300°C under an argon atmosphere. Oleylamine was used as a stabilizer solvent. Monodispersed nanoparticles up to 7.5 nm were formed [74, 75].

Adaptations from an existing route for gold nanoparticles by phase transferring were made by Tamura et al. [78]. Potassium tetrachloropalladate(II) was phase transferred into dichloromethane using tetraoctylammonium bromide before sodium borohydride reduction in the presence of optically active bidentate BINAP (2,2′-bis(-diphenylphosphino)-1,1′-binaphthyl) ligands [74, 78].

Nitrogen-based ligands, such as long-chain primary amines, are used to strongly chemically adsorb onto NPs surface. The alkyl group prevents agglomeration via steric stabilization [74]. Boron tributylamine (BTB) used in conjunction with oleylamines was presented by Sun et al. [79]. BTB was used as a coreductant and oleylamine served as a solvent, stabilizing ligand, and reductant. Several other nitrogen-based ligands have been reported, such as pyridines [80], amines [81], and imidazole derivatives [82, 83].

Surfactants have also been extensively used as stabilizers [84]. Tetra-*N*-alkylammonium halide salts are the most chosen for this purpose (examples in [85, 86]). Imidazolium-based ionic liquids are also being used, especially in biodiesel improvement. [87, 88]. The stabilization can also be achieved by incorporating PdNPs within an organic matrix, such as polymers [89], dendritic structure [90], or biomolecules (such as proteins [91], polypeptides [92], and DNA/RNA [93]).

Production of ^{103}Pd is mostly performed via ^{103}Rh(p,n)^{103}Pd nuclear reaction in a cyclotron. The highly enriched target was bombarded with protons with an electric

current for a determined amount of time. A classical route is 18 MeV protons at 200 μA beam current for 15 h [94]. After irradiation, radiochemical separation of the target is necessary. The remaining rhodium is separated from palladium-103 by an exchange resin (such as Amberlite®IR-93) in acidic conditions. After emitting mostly x-rays with an average of 21 keV, the remaining atom is now stable rhodium with 103 mass [65]. Palladium-103 is mainly produced by the proton bombardment of rhodium (^{103}Rh (p, n)^{103}Pd). The electroplating of the target can be carried out by applying either a DC constant voltage (or current) or an AC constant voltage (or current) at an elevated temperature (typically 40–60°C). Eq. (7) summarizes palladium formation and decay.

$$^{103}_{45}\mathrm{Rh} + {}^{0}_{1}\mathrm{p} \rightarrow {}^{103}_{46}\mathrm{Pd} \xrightarrow[\gamma, X^-]{} {}^{103}_{45}\mathrm{Rh} \tag{7}$$

To estimate final number of atoms formed, the following calculation is used (Eqs. 8 and 9) [17, 95] (Table 3):

$$R = n_T I \int_{E_S}^{E_0} \frac{\sigma(E)}{dE/dx} dE \tag{8}$$

$$n_T = \frac{\rho x_m}{A_T} N \tag{9}$$

Next, we will present the advances in ^{103}PdNPs reported in the literature.

Table 3 Initials meaning for Eqs. (8) and (9).[a]

Initial	Meaning	Unity
R	N	Nuclei/second Converted to activity by using Eq. (3)
n_T	The target thickness	nuclei/cm^2
I	Incident particle flux per second and is related to the beam current;	particle flux/second
N	Avogadro	6.02×10^{23}
$\boldsymbol{\sigma}$	Reaction cross-section, or probability of interaction, and is a function of energy	cm^2
E	The energy of the incident particles	eV
x	The distance traveled by the particle	cm
E_0	Initial energy of the incident particle along its path	eV
E_s^a	Final energy of the incident particle along its path	eV
A_T	Atomic weight of the target material	Grams
ρ	Density	g/cm^3
x_m	The distance the particle travels through the material	cm

[a] As the particle passes through the target material, it loses energy due to the interactions of the particle with the electrons of the target. This is represented in the above equation by the term dE/dx (also called the stopping power).

The group led by M.A. Fortin presented nanoparticles species fabrication by following the core-shell (denominated by @) pathway: PEG-^{103}Pd:Pd@AuNPs [96] and PEG-^{103}Pd:Pd@^{198}AuNPs [97]).

Basic synthesis involved the following steps:

- 0.075 mM of H_2PdCl_4 precursor solution was mixed with $^{103}PdCl_2$. Centrifugation (3000 × g, 2 min) to remove any aggregate was performed.
- The $^{103}Pd:PdCl_2$ mixture was rapidly transferred into a 0.3 mM DMSA (2,3-meso-dimercaptosuccinic acid, acting as a capping agent) solution and 30 mM ascorbic acid solution, under vigorous stirring (final NP concentration of 0.06 mM). A change from light yellow to dark brown indicated the formation of ultrasmall Pd cores.
- Then ^{103}Pd:PdNPs were used as seeds for the growth of a gold shell (Pd@Au).
- $HAuCl_4$ solution was added to the Pd nanocores suspension under stirring.
- NH2-PEG-SH was added to the solution to ensure colloidal stability. The reaction proceeded for 2 more hours, followed by centrifugation (16,000 × g, 15 min). The supernatant was discarded, and the nanoparticles were washed twice with nanopure water, followed by ultracentrifugation.
- NPs were concentrated by centrifugation into small volumes (typically: 30–60 μL).

Route for alginate-PEG-^{103}Pd:Pd@AuNPs synthesis is as follows:

- Same route, but with $H_2Pd^{103}Cl_4$ precursor in solution with 54 mL and 39.1 mCi
- The particles were centrifuge-filtered, followed by rinsing in nanopure water and two centrifugation-filtration cycles
- $HAuCl_4$ (0.5 mM) was added to Pd nanocore solution with an ascorbic acid solution (0.9 mM); Diameter was 49.5 nm
- NH2-PEG-SH was added—same procedure, $d = 84.5$ nm
- The suspension was supplemented with 20 μL of an aqueous solution of sodium alginate (2% m/v) up to a final volume of ≈55 μL (1.7 mCi/4 μL injection)

Route for alginate-PEG-^{103}Pd:Pd@^{198}AuNPs synthesis is as follows:

- The same as the first three items for alginate-PEG-^{103}Pd:Pd@AuNPs synthesis
- $HAuCl_4$ solution with $H^{198}AuCl_4$ (9.4 mCi) was mixed with 0.9 mM of ascorbic acid (d = 58.1 nm)
- NH2-PEG-SH was added, same procedure ($d = 86.2$ nm)
- The suspension was supplemented with 25 μL of an aqueous solution of sodium alginate (2% m/v) up to a final volume of ≈55 μL (1.6 mCi/4 μL injection).

To follow the characteristics of regular brachytherapy seeds (volume ranging from 2 to 4 mm^3 and radioactivity between 0.5 and 2 mCi), the NP solutions were concentrated by centrifugation until similar levels: 4 μL volumes, 1.7 mCi for PEG-^{103}Pd:Pd@AuNPs, and 1.6 mCi for PEG-^{103}Pd:Pd@^{198}AuNPs. The balance between both isotopes in the double radioactive species was ^{103}Pd ≈ 1.2 mCi to ^{198}Au ≈ 0.4 mCi. The injected concentration of Au was kept between 2 and 6 mg Au per kg of body weight of BALB/c mice. According to the authors, a small fraction only of the injected dose is expected to

transit to vasculature over time, but this quantity is not expected to lead to acute toxicity issues in vivo. To slow this process, biocompatible alginate was used. They gradually degrade over several weeks in physiological conditions due to calcium exchange. Overall, both types of nanoparticles remained massively in the tumors (>75%). Significant fractions of nanoparticles were also found in the liver (≈16%).

Since this was an initial study, tumor cells continue to multiply in the periphery, but tumor size diminished considerably (56% smaller for stable gold and 75% for radioactive gold). In the future, multiple injections of radioactive NPs will be tested [97].

Moeendarbari et al. [98] also used ^{103}Pd@Au nanoseeds as a brachytherapy agent. They report a Cu-mediated surface modification process to efficiently incorporate ^{103}Pd onto hollow gold nanoparticles (~120 nm in diameter). The authors used the electrochemistry route by using hydrogen nanobubbles that served as templates and reduce Au ions into metal Au^0. The high concentration of hydrogen molecules in the bubble boundary reduces the Au^+ ion to form Au^0 clusters. Subsequently, the metal clusters act as catalysts to trigger the autocatalytic disproportionation reaction of $Na_3Au(SO_3)_2$, which leads to the formation of a gold shell around the hydrogen bubble. The metallic gold covers the bubbles to form hollow Au nanoparticles. Anodic aluminum oxide (AAO) membrane with 300 nm diameter through channels was used inside the solution to collect nanoparticles (diameter larger than 100 nm). The AuNPs feature a 25 nm polycrystalline shell with a 50 nm hollow core.

The hollow Au nanoparticles were first coated with Cu by an electroless deposition process. Then, the Cu layer was partially (about 70%) replaced by Pd through a galvanic reaction. To prepare ^{103}Pd@Au nanoseeds, ^{103}Pd solution was added after the electroless plating of Cu. Copper can be readily replaced by less reactive metals, such as ^{103}Pd:$PdCl_2$, through a single displacement reaction in an aqueous solution containing metal ions without any other additives. The plating of ^{103}Pd was allowed to continue for 24 h upon the addition of the Pd plating solution. Exactly 3 mL of 0.1 M citric acid solution containing 4.37 mCi ^{103}Pd was added. Plating of ^{103}Pd on HAuNPs was then continued for 24 h, followed by the addition of cold Pd plating solution (containing 0.0025 M $PdCl_2$ in 0.4 M citric acid solution) to replace all Cu. After 1 h, 2 M NaOH was added to dissolve the membrane and the resultant ^{103}Pd@Au nanoseed suspension was washed thrice with water. The incorporation yield was >80%. The total synthesis time of ^{103}Pd@Au nanoseeds was approximately 26 h. They were found to be extremely stable and retain their original size even after being shelved for 2 months at 8 ± 2°C.

The resulting ^{103}Pd@Au nanoseeds as a colloidal suspension were administered by direct injection into a prostate cancer xenograft model using Severe combined immunodeficiency (SCID) mice bearing human prostate cancer tumors. PC3 cells were implanted subcutaneously; tumors were allowed to grow for 4 weeks to reach a palpable size. The injection was performed intratumorally at 6–9 locations for each tumor. The injected radioactivity was 1.5 mCi and volume under 40 μL. The gold nanoparticle

concentration in each injection was 2.03×10^{10} nanoparticles/mL. The size of the nanoseeds was large enough to prevent diffusion, resulting in >95% nanoseeds being retained inside the tumor over the entire course of the 5-week treatment. A high therapeutic efficacy was observed without noticeable side effects on the liver, spleen, and other organs. Over the 5-week treatment period, the group treated with ^{103}Pd@Au nanoseeds showed a significantly retarded tumor growth or tumor size shrinkage ($82.75 \pm 46.25\,mm^3$ to $19.83 \pm 20.12\,mm^3$).

3.4 Other nuclei

3.4.1 Indium-111

Indium-111 has a half-life of 2.8 days and emissions: γ with 245.35 KeV (94%) and 171.3 KeV (90%); and X with main emission 23 KeV [65]. It is produced by proton irradiation in a cyclotron following: (p,2n) for ^{112}Cd target or (p,n) for ^{111}Cd target [94]. Indium-111 nanoparticles have been considered as an alternative to treat HER2 breast cancer by the group led by R. M. Reilly from the University of Toronto, Canada. They have produced and tested Tras-^{111}In@AuNPs [99]. Trastuzumab (tras) is a monoclonal antibody used to treat breast cancer, specifically for HER2 receptor-positive cancer.

Briefly, 500 μg of trastuzumab in 50 μL of 100 mM $NaHCO_3$, pH 9.3 was reacted with a 25-fold molar excess of orthopyridyldisulfide-polyethyleneglycol-*N*-hydroxysuccinimide (OPSS-PEG5k-SVA) overnight at 4°C. PEGylated trastuzumab (trastuzumab-PEG-OPSS) was purified and buffer exchanged into phosphate-buffered saline (PBS), pH 7.5, by ultrafiltration. Thiolated PEG derivatized with benzylisothiocyanate diethylenetriaminepentaacetic acid (SH-PEG2k-Bn-DTPA; 10 μg) was then complexed with $^{111}InCl_3$ in 1 M sodium acetate buffer, pH 6.0 at room temperature for 30 min. The final radiochemical purity of SH-PEG2k-Bn-DTPA-^{111}In was >95. Finally, Tras-^{111}In@AuNPs were constructed by reacting 1 mL of 30 nm AuNP (2×10^{11} particles per mL) with 0.4 μg of SHPEG2k-Bn-DTPA-^{111}In (with 0.7–0.8 MBq) at 4°C for 30 min, then with 10 μg trastuzumab-PEG5k-OPSS for 5 min. Tras-^{111}In@AuNPs were finally surface-coated with an excess (7.6 μg) of PEG2k-SH for 30 min to prevent aggregation in vitro and minimize liver and spleen uptake in vivo. The final product was then purified from excess reagents by centrifugation at 2500 × g for 30 min at 4°C followed by 15,000 × g for 30 min at 4°C. The supernatant was carefully removed, and trastuzumab-AuNP-^{111}In was re-suspended in 1 mL of PBS, pH 7.5 [99].

MDA-MB-361 human breast cancer (BC) cells overexpressing HER2 were injected subcutaneously into female CD1-athymic mice. 10 MBq in 100 μL of normal saline of Tras-^{111}In@AuNPs was injected directly into cancer arresting tumor growth over a 70-day observation period. In contrast, untreated mice receiving only normal saline injections exhibited rapidly increasing tumor growth reaching 8-times their initial size over 70 days [99].

3.4.2 Lutetium-177

Lutetium-177 has also being studied as a viable isotope for use in nanobrachytherapy. It has a half-life of 6.6 days and mainly β^- emissions of 149 keV [65]. It is produced by neutron irradiation in a nuclear reactor [94]. The main methods for producing ^{177}Lu of high specific activity are based on irradiation of either ^{176}Lu or ^{176}Yb with reactor neutrons following Eqs. (10) and (11) [100]:

$$^{176}_{71}\mathrm{Lu} + {}^{1}_{0}\mathrm{n} \rightarrow {}^{177}_{71}\mathrm{Lu} \xrightarrow[\gamma, X, \beta^-]{} {}^{177}_{72}\mathrm{Hf} \tag{10}$$

$$^{176}_{70}\mathrm{Yb} + {}^{1}_{0}\mathrm{n} \rightarrow {}^{177}_{71}\mathrm{Lu} \xrightarrow[\gamma, X, \beta^-]{} {}^{177}_{72}\mathrm{Hf} \tag{11}$$

Lutetium-177 gold nanoparticles were also considered by R.M. Reilly research group as an alternative to treat HER2 breast cancer. They have produced and tested Tras-^{177}Lu@AuNPs [101]. The methodology is as follows: Tras-^{177}Lu@AuNPs were constructed by stepwise incubation of 2×10^{11} AuNPs (30 nm) in 1 mL of 20 mM $NaHCO_3$, pH 9.0 at 4°C with:

- OPSS-PEG-DOTA consisted of polyethylene glycol (4 kDa) functionalized with ortho-pyridyl disulfide (OPSS) at one end to create a gold-sulfur bond and at the opposite end with a 1,4,7,10- tetraazacyclododecane-1,4,7,10-tetraacetic acid (DOTA) that acts as a chelator to complex ^{177}Lu (full description in [102]—Supporting information).
- Labeling with ^{177}Lu was carried out by incubation with $^{177}LuCl_3$ in 1 M sodium acetate buffer, pH 4.5 at 80°C for 30 min. The final radiochemical purity of OPSS-PEG3k-DOTA-^{177}Lu was >95%.
- OPSS-PEG5k-trastuzumab was prepared by reacting trastuzumab (200 μg) with a 5-fold molar excess of OPSS-PEG5k-succinimidyl valerate (SVA) in 100 mM $NaHCO_3$ buffer, pH 9.3 overnight at 4°C. Trastuzumab-PEG5k-OPSS was purified and buffer-exchanged into Milli-Q® water by ultrafiltration.
- No details on how OPSS-PEG3k-DOTA-^{177}Lu reaction with OPSS-PEG5k-trastuzumab to result in OPSS-PEG5k-trastuzumab-DOTA-^{177}Lu were reported.
- Following each step, AuNP were centrifuged at 15,000 × g for 15 min at 4°C to remove unreacted ligands [101].

MDA-MB-361 human breast cancer (BC) cells overexpressing HER2 were injected subcutaneously into female NOD/SCID mice. 20 MBq to 1 mg AuNP in normal saline of Tras-^{111}In@AuNPs was injected directly into cancer significantly inhibiting tumor growth during the 16 days observation period [101]. However, tumor growth arrest was not achieved with Trastuzumab.

A similar study was performed by the same group but with panitumumab [102]. The mass number of NPs injected in these two studies was the same, but the radioactivity injected in the trastuzumab [101] study was one-third lower (3.0 vs. 4.5 MBq). Tumor

arrest was achieved in MDA-MB-468 cells with panitumumab. The group is expanding both studies.

Vilchis-Juárez et al. demonstrated that 20 nm diameter AuNP labeled with ^{177}Lu targeted to α(v)β(3)-integrin-positive C6 glioma was able to deposit high radiation doses (>60 Gy) in xenografts in mice preventing tumor progression [103]. The cysteine in DOTA-GGC (1,4,7,10-tetraazacyclododecane-*N*′,*N*″,*N*‴-tetraacetic-Gly-Gly-Cys) molecule is used to interact with the gold nanoparticle surface and DOTA is used as the lutetium-177 chelator. A 5 μL aliquot of DOTA-GGC (1 mg/mL) was diluted with 40 μ of 1 M acetate buffer at pH 5, followed by the addition of 10 μL of a $^{177}LuCl_3$ solution. The mixture was incubated at 90°C in a block heater for 30 min. Separately, to 1 mL of AuNP (20 nm), 0.025 mL of c[RGDfK(C)] (Arg-Gly-Asp cyclo peptide) was added, followed by 3 μL (40 MBq) of 177Lu-DOTA-GGC, and the mixture was stirred for 5 min to form the ^{177}Lu-DOTA-GGC-AuNP-c[RGDfK(C)]. The complex has 2 MBq/0.05 mL was injected intratumorally. High tumor retention was observed (68%). The rest of the activity occurred mainly in the kidneys and liver, as well as in the spleen, with negligible uptake in other organs. In the end, significantly decreased glioma tumor progression in mice through the effect of a combined molecular targeting therapy/radiotherapy was observed.

4. Conclusion

With the rapid increase in cancer occurrence, new forms of treatment are and must be investigated. Also, easy and portable forms are of the utmost importance. Nanoseeds-based brachytherapy fits perfectly with these conditions, with the potential of:

- bringing effective and easy treatment to remote areas
- enabling effective treatment of smaller tumors: procedure can be performed intraoperatively when optimal surgical resection is not possible
- completely halt cancer growth or significantly diminish its size
- controlling nanoseeds size to prevent diffusion, focusing radiation effects on the target

This chapter presented the basics of radiation physics and the routes being investigated to produce radioactive nanoparticles. Efforts have been made mostly with gold-198, palladium-106, indium-111, and lutetium-177. Practically, all results reported were successful in cancer progression halt or even completely cancer cure. The potential is huge since the treatment is injectable and radiation activity is considerably low.

Necrosis was found in the skin of the animals injected with alginate-PEG-^{103}Pd:Pd@^{198}AuNPs [97]. This is due to gold-198 high gamma emission energy. Necrosis confirms the impact of the treatment on tumor volume control but elucidates the difficulty of circumspect the radiotherapeutic treatment to the exact site of the tumor tissue.

There are still several steps that need to be developed so that nanobrachytherapy can be implemented on large scale. They are:

(a) Stability tests: radioactive nanoparticles need to be proven stable from the production line to the treatment place.

(b) Mercury contamination assay: gold-198 decays to mercury, which is highly toxic. Effects of this on the cells are yet to be evaluated.

(c) Nanotoxicity: evaluation of the toxicity level of nonradioactive nanoparticle counterparts needs detailed investigation.

(d) More in vitro testing: a complete assessment of inflammatory and immunity response needs further evaluation.

(e) More in vivo testing: by evaluating possible routes and understanding the nanomaterials transport it will be possible to evaluate the distribution of radioactive nanoparticles in the human body after systemic administration and reproducible demonstration of the therapeutic efficiency.

(f) Dosimetry: it is imperative that models are created that can accurately measure radiation dose delivered to the target and healthy surrounding tissues. Protocols comprising of different dosimetry studies, simulation-based dosimetry systems, and computer treatment planning systems must be investigated/created.

(g) Industrial or semi-industrial laboratory construction: tabletop research is very important because it validates the technique. However, fabrication on a large-scale, to provide to hospitals and clinics, is a different issue on its own. Methods that are too complicated may not be translated to an industrial scale. Also, these new products need to be produced with the highest level of precision under good manufacturing practices and by respecting radiation protection demands.

Even with all these challenges, some non-radioactive NPs are being investigated in clinical studies for cancer treatment. On the U.S. National Library of Medicine website (www.clinicaltrials.gov) a list of compounds in different stages (Phase I, II, and III oncology studies) can be found. As an example, AuroLase (NCT02680535) is a therapy project by Nanospectra Biosciences based on PEG-Si@AuNPs, that uses focal ablation of neoplastic prostate tissue via nanoparticle directed irradiation. Although not radioactive, these clinical studies open the door to more clinical investigations in the field, including with radioactive NPs. For nanobrachytherapy to become a viable technique, besides the higher monetary investment in this area of research, there is no doubt that interdisciplinary teams are of the utmost necessity.

References

[1] ScienceDirect, Nanoparticle search engine results, 2019 (cited 2019 Sept. 24).
[2] Alves, O.L., Cartilha sobre nanotecnologia, Agencia Brasileira de Desenvolvimento Industrial, Editor. 2011: Brasília.
[3] C. Daruich De Souza, B. Ribeiro Nogueira, M.E.C.M. Rostelato, Review of the methodologies used in the synthesis gold nanoparticles by chemical reduction, J. Alloys Compd. 798 (2019) 714–740.

[4] M. Adams, Nanoparticles Technology Handbook, first ed., NY Research Press, New York, 2015, p. 346.
[5] M.-C. Daniel, D. Astruc, Gold Nanoparticles: assembly, supramolecular chemistry, quantum-size-related properties, and applications toward biology, catalysis, and nanotechnology, Chem. Rev. 104 (1) (2004) 293–346.
[6] D.R. Baer, et al., Surface characterization of nanomaterials and nanoparticles: Important needs and challenging opportunities, J. Vacuum Sci. Technol. A, Vacuum, Surf. Films: Off. J. Am. Vacuum Soc. 31 (5) (2013) 50820.
[7] J. Zhao, M.H. Stenzel, Entry of nanoparticles into cells: the importance of nanoparticle properties, Polym. Chem. 9 (3) (2018) 259–272.
[8] M.E.C.M. Rostelato, et al., Surface coating and study of metallic cores for radioactive sources production used in cancer treatment, in: International Conference on Advanced Material Science and mechanic engineering –AMSME, Bangkok, 2016.
[9] A.S.M. Thorn, The Impact of Nanoparticle Surface Chemistry on Biological Systems, University of Iowa, 2017. p. 136.
[10] H.E. Toma, et al., The coordination chemistry at gold nanoparticles, J. Braz. Chem. Soc. 21 (2010) 1158–1176.
[11] E.B. Podgorsak, Radiation Oncology Physics: A Handbook for Teachers and Students, first ed., International Atomic Energy Agency, Viena, 2005.
[12] C.D. de Souza, Materials for the course: TNA 5744 dicipline—Applications of Intense Radiation Sources, 2019.
[13] C.D. de Souza, Materials for the course: TNA5805 Brachytherapy: Fundamentals, Production, Application, Dosimetry and Quality, 2019.
[14] C.D. de Souza, et al., New gold-198 nanoparticle synthesis to be used in cancer treatment, Brazilian J. Radiat. Sci. 9 (01-A) (2021) 18.
[15] C.D. de Souza, et al., New core configuration for the fabrication of 125I radioactive sources for cancer treatment, Appl. Radiat. Isot. 165 (2020) 109307.
[16] W.E. Meyerhof, Elements of Nuclear Physics, McGraw-Hill Book Company, New York, 1989.
[17] E.F. Pessoa, F.A.B. Coutinho, O. Sala, Introdução à Física Nuclear, Editora da Universidade de São Paulo/McGraw-Hill-Brasil, São Paulo, 1978.
[18] Departamento de Física Nuclear. Instituto de Física da Universidade de São Paulo, Decaimento Alfa, 2019 (cited 2019 Sept, 25).
[19] Berkeley Lab, Alpha Decay. Guide to Nuclear Wallchart 2000, 2000 (cited 2019 25 sept).
[20] Departamento de Física Nuclear. Instituto de Física da Universidade de São Paulo, Decaimento Beta, 2019 (cited 2019 Sept, 25).
[21] Berkeley Lab, Beta Decay. Guide to Nuclear Wallchart 2000, 2000 (cited 2019 25 sept).
[22] Departamento de Física Nuclear. Instituto de Física da Universidade de São Paulo, Decaimento Gama, 2019 (cited 2019 Sept, 25).
[23] Berkeley Lab, Gamma Decay. Guide to Nuclear Wallchart 2000, 2000 (cited 2019 Sept 25).
[24] F.A. Mettler Jr., A.C. Upton, Medical Effects of Ionizing Radiation, 2nd, Saunders, Philadelphia, PA, 1995.
[25] N. Nishida, et al., Angiogenesis in cancer, Vasc. Health Risk Manag. 2 (3) (2006) 213–219.
[26] L. Holmgren, M.S. O'Reilly, J. Folkman, Dormancy of micrometastases: balanced proliferation and apoptosis in the presence of angiogenesis suppression, Nat. Med. 1 (2) (1995) 149–153.
[27] S. Parangi, et al., Antiangiogenic therapy of transgenic mice impairs de novo tumor growth, Proc. Natl. Acad. Sci. U. S. A. 93 (5) (1996) 2002–2007.
[28] E.B. Podgorsak, Radiation Oncology Physics: A Handbook For Teachers And Students, International Atomic Energy Agency, Viena, 2005.
[29] Centro de Tecnologia das Radiações—IPEN, et al., Relatório Técnico 01—Acordo Baterias Nucleares, Instituto de Pesquisas Energéticas e Nucleares, 2019.
[30] L. Beaulieu, et al., Report of the Task Group 186 on model-based dose calculation methods in brachytherapy beyond the TG-43 formalism: Current status and recommendations for clinical implementation (Task Group No. 186), Med. Phys. 39 (10) (2012) 28.

[31] A.V. Rane, et al., Chapter 5—Methods for synthesis of nanoparticles and fabrication of nanocomposites, in: S.M. Bhagyaraj, et al. (Eds.), Synthesis of Inorganic Nanomaterials, Woodhead Publishing, 2018, pp. 121–139.
[32] J. Polte, Fundamental growth principles of colloidal metal nanoparticles—a new perspective, CrstEngComm 17 (36) (2015) 6809–6830.
[33] Turkevich, J., P.C. Stevenson, and J. Hillier, A study of the nucleation and growth processes in the synthesis of colloidal gold. Discuss. Faraday Soc., 1951. 11(0): p. 55–75.
[34] P. Kalimuthu, S.A. John, Studies on ligand exchange reaction of functionalized mercaptothiadiazole compounds onto citrate capped gold nanoparticles, Mater. Chem. Phys. 122 (2–3) (2010) 380–385.
[35] C.R. Raj, T. Okajima, T. Ohsaka, Gold nanoparticle arrays for the voltammetric sensing of dopamine, J. Electroanal. Chem. 543 (2) (2003) 127–133.
[36] M. Brust, G.J. Gordillo, Electrocatalytic hydrogen redox chemistry on gold Nanoparticles, J. Am. Chem. Soc. 134 (7) (2012) 3318–3321.
[37] M. Brust, et al., Synthesis of thiol-derivatised gold nanoparticles in a two-phase Liquid-Liquid system, J. Chem. Soc. Chem. Commun. 7 (1994) 801–802.
[38] N.R. Jana, L. Gearheart, C.J. Murphy, Seeding growth for size control of 5 – 40 nm diameter gold Nanoparticles, Langmuir 17 (22) (2001) 6782–6786.
[39] A.S. Patel, et al., Gold nanoflowers as efficient hosts for SERS based sensing and bio-imaging, Nano-Struct. Nano-Obj. 16 (2018) 329–336.
[40] Sonia, et al., Exploring the DNA damaging potential of chitosan and citrate-reduced gold nanoparticles: Physicochemical approach, Int. J. Biol. Macromol. 115 (2018) 801–810.
[41] M.S. Bakshi, How surfactants control crystal growth of nanomaterials, Cryst. Growth Des. 16 (2) (2016) 1104–1133.
[42] S. Kumar, Role of Surfactants in Synthesis and Stabilization of Nanoparticles Spectroscopic and Physicochemical Aspects, Panjab University, 2011. p. 218.
[43] S.B. Awan, et al., Historical review of interstitial prostate brachytherapy, Int. J. Radiat. Res. 5 (4) (2008) 153–168.
[44] Science and Technology Branch, in: H.G. Donald (Ed.), Bibliography from Nuclear Science Abstracts, Vol. 21, United States Atomic Energy Commission, 1968. https://books.googleusercontent.com/books/content?req=AKW5QafMlZ0ZqnEcNom8f20jjXeJwvLqUOCfxkXl4IP8IMtStBNSsZPlZ5Srry_zoXqQ3RjJ2pwlSXbFJxp6RuuP84wbPjjzDbhilJ6zUPAGZdd27rumDeonrsaJZaW4vsh0GNJ7Ah-C-plbQIVNJAibCe2Rf86SEfgjFDv4KuXPLV08gxKAvtr2fuJNSrdPupZRimYBhVKbn83BLOvkwKl3gKvwcpc_TOJ5vHpzFeZAW1aOjB5QV1ulX48Dm81LZFHmBVQ0xervAoeUhRurszB3gTte4Qdirg.
[45] C.D. Souza, et al., New Gold-198 nanoparticle synthesis to be used in cancer treatment, in: 60th AAPM Annual Meeting and Exhibition, Nashville, USA, 2018.
[46] I. Freestone, et al., The Lycurgus cup—a Roman nanotechnology, Gold Bull. 40 (4) (2007) 270–277.
[47] L.A. Dykman, N.G. Khlebtsov, Gold nanoparticles in biology and medicine: recent advances and prospects, Acta Nat. 3 (2) (2011) 34–55.
[48] J.J. Storhoff, et al., Gold nanoparticle-based detection of genomic DNA targets on microarrays using a novel optical detection system, Biosens. Bioelectron. 19 (8) (2004) 875–883.
[49] Y. Li, H.J. Schluesener, S. Xu, Gold nanoparticle-based biosensors, Gold Bull. 43 (1) (2010) 29–41.
[50] X. Liu, et al., A one-step homogeneous immunoassay for cancer biomarker detection using gold nanoparticle probes coupled with dynamic light scattering, J. Am. Chem. Soc. 130 (9) (2008) 2780–2782.
[51] P.V. Baptista, et al., Gold-nanoparticle-probe-based assay for rapid and direct detection of *Mycobacterium tuberculosis* DNA in clinical samples, Clin. Chem. 52 (7) (2006) 1433–1434.
[52] Y. Cheng, et al., Highly efficient drug delivery with gold nanoparticle vectors for in vivo photodynamic therapy of cancer, J. Am. Chem. Soc. 130 (32) (2008) 10643–10647.
[53] S. Thambiraj, S. Hema, D. Ravi Shankaran, Functionalized gold nanoparticles for drug delivery applications, Mater. Today: Proc. 5 (8, Part 3) (2018) 16763–16773.

[54] W. Lu, et al., Gold nano-popcorn-based targeted diagnosis, nanotherapy treatment, and in situ monitoring of photothermal therapy response of prostate cancer cells using surface-enhanced Raman spectroscopy, J. Am. Chem. Soc. 132 (51) (2010) 18103–18114.
[55] M. Faraday, The Bakerian lecture: experimental relations of gold (and other metals) to light, Philos. Trans. R. Soc. Lond. A 147 (1857) 145–181.
[56] S. Jain, D.G. Hirst, J.M. O'Sullivan, Gold nanoparticles as novel agents for cancer therapy, Br. J. Radiol. 85 (1010) (2012) 101–113.
[57] P.F. Hahn, et al., Intravenous radioactive gold in the treatment of chronic leukemia, Acta Radiol. 50 (6) (1958) 565–572.
[58] Hahn, P.F. and E.L. Carothers, Use of radioactive colloidal metallic gold in the treatment of malignancies. Nucleonics, 1950. 6(1): p. 54–62, illust.
[59] P.F. Hahn, J.P. Goodell, et al., Direct infiltration of radioactive isotopes as a means of delivering ionizing radiation to discrete tissues, J. Lab. Clin. Med. 32 (12) (1947) 1442–1453.
[60] J.H. Muller, Medical therapeutic use of artificial radioactivity, Bull. Schweiz. Akad. Med. Wiss. 5 (5–6) (1949) 484–510.
[61] P.C. Lee, D. Meisel, Adsorption and surface-enhanced Raman of dyes on silver and gold sols, J. Phys. Chem. 86 (17) (1982) 3391–3395.
[62] N. Chanda, et al., Radioactive gold nanoparticles in cancer therapy: therapeutic efficacy studies of GA-198AuNP nanoconstruct in prostate tumor-bearing mice, Nanomedicine 6 (2) (2010) 201–209.
[63] X. Chen, et al., Formation and catalytic activity of spherical composites with surfaces coated with gold nanoparticles, J. Colloid Interface Sci. 322 (2) (2008) 414–420.
[64] C.D. de Souza, Relatório de Pós-Doutorado, Instituto de Pesquisas Energéticas e Nucleares, 2019.
[65] International Atomic Nuclear Agency, Live Chart of Nuclides: nuclear structure and decay data, 2019 (cited 2020, 26 Feb).
[66] K.V. Katti, et al., Hybrid gold nanoparticles in molecular imaging and radiotherapy, Czechoslov. J. Phys. 56 (4) (2006) D23–D34.
[67] R. Shukla, et al., Laminin receptor specific therapeutic gold nanoparticles (198AuNP-EGCg) show efficacy in treating prostate cancer, Proc. Natl. Acad. Sci. U. S. A. 109 (31) (2012) 12426–12431.
[68] N. Rao, et al., Isolation of a tumor cell laminin receptor, Biochem. Biophys. Res. Commun. 111 (3) (1983) 804–808.
[69] J.C. Blasko, et al., Palladium-103 brachytherapy for prostate carcinoma, Int. J. Radiat. Oncol. Biol. Phys. 46 (4) (2000) 839–850.
[70] K.R. Gopidas, J.K. Whitesell, M.A. Fox, Synthesis, characterization, and catalytic applications of a palladium-nanoparticle-cored dendrimer, Nano Lett. 3 (12) (2003) 1757–1760.
[71] Y.E. Cheon, M.P. Suh, Enhanced hydrogen storage by palladium nanoparticles fabricated in a redox-active metal-organic framework, Angew. Chem. Int. Ed. 48 (16) (2009) 2899–2903.
[72] X.-M. Chen, et al., Nonenzymatic amperometric sensing of glucose by using palladium nanoparticles supported on functional carbon nanotubes, Biosens. Bioelectron. 25 (7) (2010) 1803–1808.
[73] J. Cookson, The preparation of palladium nanoparticles, Platin. Met. Rev. 56 (2) (2012) 83–98.
[74] J. Cookson, The preparation of palladium nanoparticles, Platinum Met. Rev. 56 (2) (2012) 15.
[75] S.-W. Kim, et al., Synthesis of monodisperse palladium nanoparticles, Nano Lett. 3 (9) (2003) 1289–1291.
[76] C.K. Yee, et al., Novel one-phase synthesis of thiol-functionalized gold, palladium, and iridium Nanoparticles using Superhydride, Langmuir 15 (10) (1999) 3486–3491.
[77] D.E. Cliffel, et al., Mercaptoammonium-monolayer-protected, water-soluble gold, silver, and palladium clusters, Langmuir 16 (25) (2000) 9699–9702.
[78] M. Tamura, H. Fujihara, Chiral Bisphosphine BINAP-stabilized gold and palladium nanoparticles with small size and their palladium nanoparticle-catalyzed asymmetric reaction, J. Am. Chem. Soc. 125 (51) (2003) 15742–15743.
[79] V. Mazumder, S. Sun, Oleylamine-mediated synthesis of Pd nanoparticles for catalytic formic acid oxidation, J. Am. Chem. Soc. 131 (13) (2009) 4588–4589.
[80] H. Shen, et al., Novel glycosyl pyridyl-triazole@ palladium nanoparticles: efficient and recoverable catalysts for C–C cross-coupling reactions, Cat. Sci. Technol. 5 (4) (2015) 2065–2071.

[81] R.A. Molla, et al., Mesoporous poly-melamine-formaldehyde stabilized palladium nanoparticle (Pd@mPMF) catalyzed mono and double carbonylation of aryl halides with amines, RSC Adv. 4 (89) (2014) 48177–48190.
[82] Y.M. Yamada, S.M. Sarkar, Y. Uozumi, Self-assembled poly (imidazole-palladium): highly active, reusable catalyst at parts per million to parts per billion levels, J. Am. Chem. Soc. 134 (6) (2012) 3190–3198.
[83] S.M. Sarkar, Y. Uozumi, Y.M. Yamada, A highly active and reusable self-assembled poly (imidazole/palladium) catalyst: allylic Arylation/Alkenylation, Angew. Chem. Int. Ed. 50 (40) (2011) 9437–9441.
[84] D. Astruc, Palladium nanoparticles as efficient green homogeneous and heterogeneous carbon−-carbon coupling precatalysts: a unifying view, Inorg. Chem. 46 (6) (2007) 1884–1894.
[85] W. Kleist, J.K. Lee, K. Köhler, Pd/MOx materials synthesized by sol-gel Coprecipitation as catalysts for carbon–carbon coupling reactions of aryl bromides and chlorides, Eur. J. Inorg. Chem. 2009 (2) (2009) 261–266.
[86] J. Bennett, et al., Nanoparticles of palladium supported on bacterial biomass: new re-usable heterogeneous catalyst with comparable activity to homogeneous colloidal Pd in the heck reaction, Appl. Catal. Environ. 140 (2013) 700–707.
[87] M.S. Carvalho, et al., In situ generated palladium nanoparticles in imidazolium-based ionic liquids: a versatile medium for an efficient and selective partial biodiesel hydrogenation, Cat. Sci. Technol. 1 (3) (2011) 480–488.
[88] B.S. Souza, et al., Selective partial biodiesel hydrogenation using highly active supported palladium nanoparticles in imidazolium-based ionic liquid, Appl. Catal. A. Gen. 433 (2012) 109–114.
[89] S. Jones, et al., Prominent electronic and geometric modifications of palladium nanoparticles by polymer stabilizers for hydrogen production under ambient conditions, Angew. Chem. Int. Ed. 51 (45) (2012) 11275–11278.
[90] L. Wu, et al., Phosphine dendrimer-stabilized palladium nanoparticles, a highly active and recyclable catalyst for the Suzuki-Miyaura reaction and hydrogenation, Org. Lett. 8 (16) (2006) 3605–3608.
[91] A. Prastaro, et al., Suzuki-Miyaura cross-coupling catalyzed by protein-stabilized palladium nanoparticles under aerobic conditions in water: application to a one-pot chemoenzymatic enantioselective synthesis of chiral biaryl alcohols, Green Chem. 11 (12) (2009) 1929–1932.
[92] G. Marcelo, A. Muñoz-Bonilla, M. Fernández-García, Magnetite-polypeptide hybrid materials decorated with gold nanoparticles: study of their catalytic activity in 4-nitrophenol reduction, J. Phys. Chem. C 116 (46) (2012) 24717–24725.
[93] L.A. Gugliotti, D.L. Feldheim, B.E. Eaton, RNA-mediated metal-metal bond formation in the synthesis of hexagonal palladium nanoparticles, Science 304 (5672) (2004) 850–852.
[94] International Atomic Energy Agency, Technical Reports Series No. 468: Cyclotron Produced Radionuclides: Physical Characteristics and Production Methods, 2009. https://www-pub.iaea.org/MTCD/publications/PDF/trs468_web.pdf.
[95] International Atomic Energy Agency, Cyclotron Produced Radionuclides: Physical Characteristics And Production Methods, 2009. p. 2009.
[96] D. Djoumessi, et al., Rapid, one-pot procedure to synthesise 103Pd:Pd@au nanoparticles en route for radiosensitisation and radiotherapeutic applications, J. Mater. Chem. B 3 (10) (2015) 2192–2205.
[97] M. Laprise-Pelletier, et al., Low-dose prostate cancer brachytherapy with radioactive palladium-gold nanoparticles, Adv. Healthc. Mater. 6 (4) (2017) 24.
[98] S. Moeendarbari, et al., Theranostic Nanoseeds for efficacious internal radiation therapy of Unresectable solid tumors, Sci. Rep. 6 (2016) 20614.
[99] Z. Cai, et al., 111In-labeled trastuzumab-modified gold nanoparticles are cytotoxic in vitro to HER2-positive breast cancer cells and arrest tumor growth in vivo in athymic mice after intratumoral injection, Nucl. Med. Biol. 43 (12) (2016) 818–826.
[100] R.A. Kuznetsov, et al., Production of Lutetium-177: process aspects, Radiochemistry 61 (4) (2019) 381–395.
[101] Z. Cai, et al., Local radiation treatment of HER2-positive breast cancer using Trastuzumab-modified gold Nanoparticles labeled with 177Lu, Pharm. Res. 34 (3) (2017) 579–590.

[102] S. Yook, et al., Radiation nanomedicine for EGFR-positive breast Cancer: Panitumumab-modified gold Nanoparticles complexed to the β-particle-emitter, 177Lu, Mol. Pharm. 12 (11) (2015) 3963–3972.
[103] A. Vilchis-Juarez, et al., Molecular targeting radiotherapy with cyclo-RGDFK(C) peptides conjugated to 177Lu-labeled gold nanoparticles in tumor-bearing mice, J. Biomed. Nanotechnol. 10 (3) (2014) 393–404.